Circularly polarised equilateral triangular patch array antenna for mobile satellite communications

J.T. Sri Sumantyo and K. Ito

Abstract: A satellite-tracking left-handed circularly polarised triangular-patch array antenna has been developed to support the next generation of mobile satellite communications using Japanese Engineering Test Satellite VIII. The targeted minimum gain of the antenna was set to 5 dBic at an elevation of 48° in the Tokyo area, for applications of about a hundred kbit/s data transfer. The antenna is composed of three equilateral triangular patches and fed by a dual-proximity feed. The influence of the array configuration on the characteristic of this antenna is investigated using a method of moments (MoM) approach and a simple point source model. The measurement of the fabricated antenna was then performed to confirm the simulation results. The result showed that the 10 mm distance between the patch apex to the centre of the array antenna satisfies the target. The frequency characteristic of the fabricated antenna is 0.7% shifted to the higher frequency, and the maximum gain is 0.9 dB lower than the simulation results. The result also shows that the characteristic of the patch array antenna satisfies the specification at elevation angle $El = 48°$, especially the 5 dBic gain coverage of the results covers the whole azimuth angle in a conical-cut plane at $El = 48°$.

1 Introduction

The geostationary satellite called Engineering Test Satellite VIII (ETS-VIII) is scheduled to be launched by the Japan Aerospace Exploration Agency (JAXA). ETS-VIII will conduct orbital experiments on mobile satellite communications at the S band frequency, especially to support the development of a technology for multimedia information, such as voice and images for land mobile systems [1]. Up to now, various antennas have been developed for mobile satellite communications purposes [2–5], but these antennas have a complex composition. Hence, in this research, a simple satellite-tracking triangular-patch array antenna is proposed. The targeted minimum gain of the antenna is set to 5 dBic at an elevation of 48° in the Tokyo area for applications of a hundred kbit/s data transfer. The antenna is designed as thin, compact, small and simple as possible, because it could be mounted on a small boat or on a car roof [6]. In the future, this antenna will be applied to the multimedia service (television, radio, disaster information system etc.) inside the transportation facility, especially a car.

IEE Proceedings online no. 20050032

doi:10.1049/ip-map:20050032

Paper first received 10th February 2005 and in final revised form 3rd May 2006

J.T. Sri Sumantyo is with the Centre for Environmental Remote Sensing, Chiba University, 1-33, Yayoi, Inage, Chiba 263-8522, Japan and also with the Centre for Remote Sensing, Institute of Technology Bandung, Jalan Ganesha 10, Bandung 40132, Indonesia

K. Ito is with the Graduate School of Science and Technology, Chiba University, 1-33, Yayoi, Inage, Chiba 263-8522, Japan

E-mail: jtetukoss@faculty.chiba-u.jp

2 Antenna configuration and the mechanism of beam switching

Table 1 shows the specifications and targets of the antenna for mobile satellite communications aiming at ETS-VIII applications that are used in this research. Here, a thin miniaturised antenna designed for a hundred kbit/s data transfer required (gain of 5 dBic) is simulated using the method of moments (MoM) (IE3D Zeland Software Inc.). In addition, the measurements are assumed to take place in the centre of Tokyo, as a result the targeted elevation angle *El* is set to 48°. At first, the operating frequency of a single patch is set to 2.5025 GHz (see Table 1), then the antenna is composed in a sequential array configuration to realise a simple switching technique to track the satellite position. It is fabricated using a conventional substrate (relative permittivity $\varepsilon_r = 2.17$ and $\tan\delta = 0.00085$) and measured to confirm the simulation results.

Figure 1*a* shows the configuration of a single equilateral triangular patch with its parameters. Figure 1*b* shows the configuration of the triangular patch array antenna that is composed of three triangular elements. This configuration is used to realise a compactness. The elements are fed by proximity feeds with microstriplines whose width w is

Table 1: Specifications and targets on the antenna for mobile satellite communication (ETS-VIII)

Specifications	
Frequency	2.5005 to 2.5030 GHz
Polarisation	left-handed circular polarisation (LHCP)
Targets	
Elevation angle (*El*)	48° (Tokyo)
Azimuth angle (*Az*)	0° to 360°
Minimum gain	5 dBic
Maximum axial ratio	3 dB

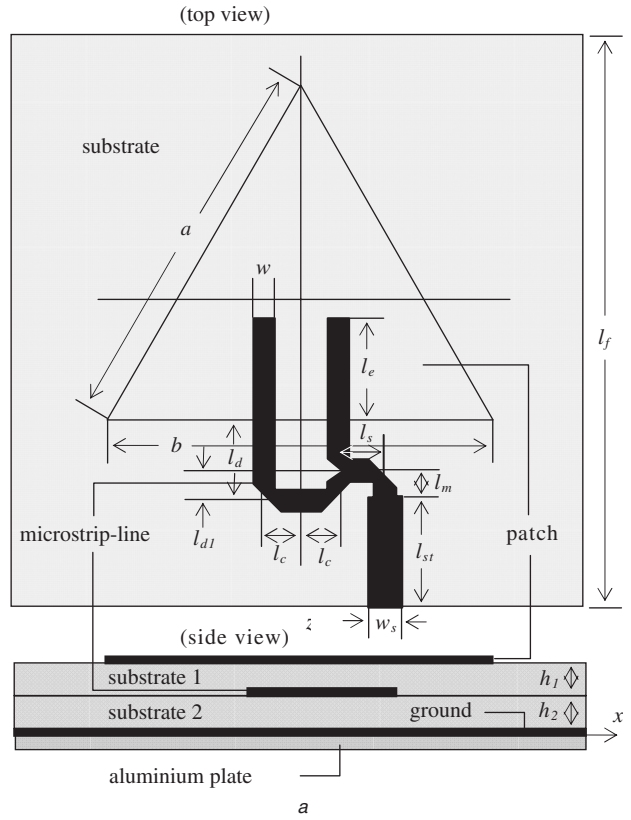

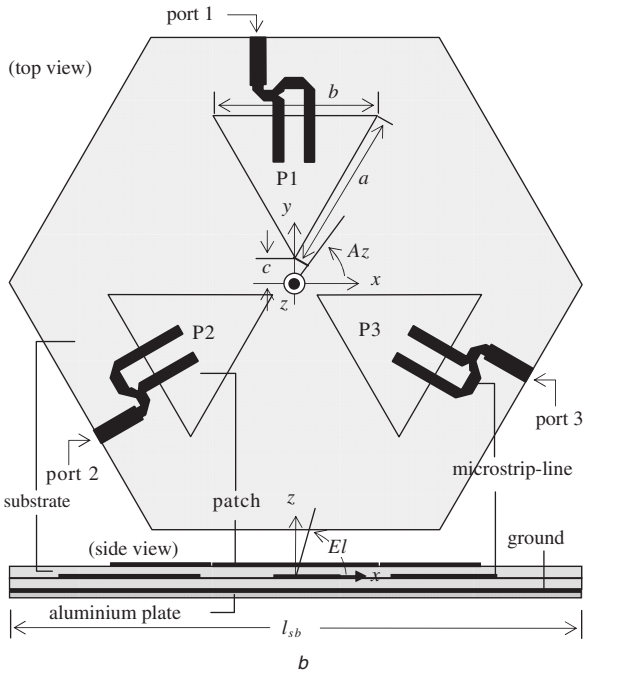

Fig. 1 *Configuration of the antenna: an equilateral triangular patch array antenna*
a Single element
b Array configuration

3.0 mm, for each patch, to obtain a thin configuration. The dual feed type is proposed to generate a left-handed circular polarisation (LHCP), where one part of the microstripline is $\lambda/4$ longer than the other microstripline to induce a 90° phase delay. In the same manner, the right-handed circular polarisation (RHCP) can be realised by changing the microstripline into the opposite configuration. The proposed feed technique is designed to obtain a stable current distribution on the triangular patch surface and the wide 3 dB coverage of axial ratio, further improving the previous developed antenna [7, 8].

Several types of circularly polarised triangular antennas have been developed [9–13], but they are difficult to design and optimise, because the ratio between *a* and *b* (see Fig. 1), sensitively affects the performance of the axial ratio. Then, the pin feed technique is commonly applied to generate a circular polarisation with a triangular antenna, but this technique is more complicated than the microstripline or proximity feed technique in the fabrication process. Additionally, this pin feed technique with a single feed point will generate an unstable current distribution on each patch, where the patches are composed in an array configuration. Thus, by using a microstripline as shown in Fig. 1, for equilateral triangular patches, it is easier to design and fabricate without any optimisation of the ratio between *a* and *b*.

In this research, the MoM was employed to investigate the characteristics of the model with a finite groundplane in array configuration. The total thickness of antenna is 1.6 mm, where the substrate thicknesses for the triangular patch (substrate 1 in Fig. 1*a*, h_1) and the microstripline (substrate 2 in Fig. 1*a*, h_2) are 0.8 mm. The length of the microstripline inserted under the patch, l_e, is 14 mm, and a quarterwave transformer is used to obtain a matching impedance of 50 Ω . Then the microstriplines are fed by an SMA connector on the edge of the substrate. The detail parameters of the microstripline are $l_s = 5$ mm, $l_d = 11$ mm, $l_{d1} = 4$ mm, $l_c = 5$ mm, $l_m = 2$ mm, $l_{st} = 11$ mm and $w_s =$ 4.7 mm (see Fig. 1*a*). The patch lengths are optimised by using a single patch. Finally, the patch length parameters ($a = b$) are obtained as 52.5 mm.

Figures 1*b* and 2 show the array configuration and the fabricated triangular-patch array antenna as top view and side view. The beam switching of the antenna to track the satellite position electronically is generated by a simple mechanism that consists in switching OFF one of the

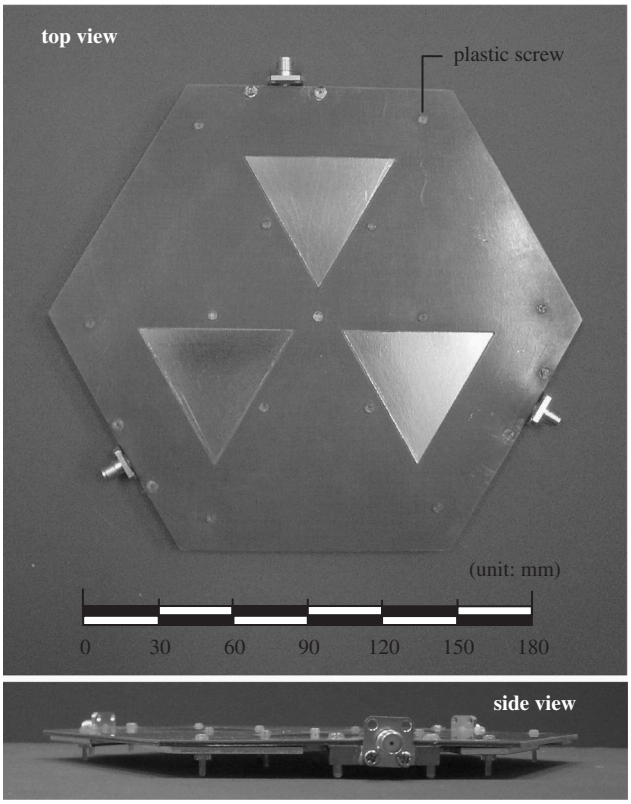

Fig. 2 *Fabricated antenna*

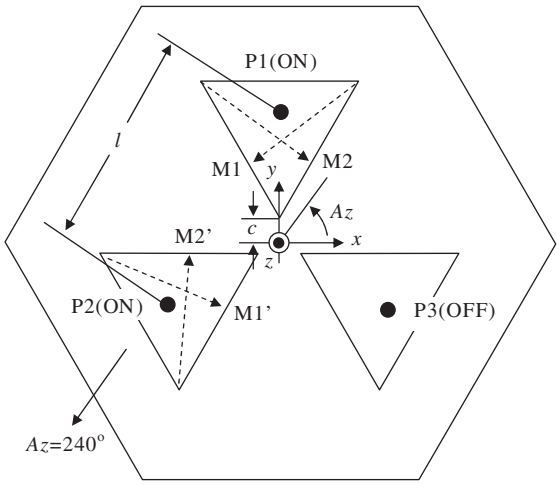

Fig. 3 *Beam generation model of equilateral triangular patch array antenna using point source model*

radiating element shown in Fig. 1*b*. By considering the mutual coupling between fed elements, and their phase and distance, the beam direction can be varied. The two fed elements theoretically generate a beam shifted -90° in the conical-cut direction from the element, which is switched OFF, in the case of an LHCP antenna. For example, when element 3 (P3) is switched OFF, the beam is theoretically directed towards the azimuth angle $Az = 240^\circ$ (see Fig. 13, beam number 3, shown as symbol ♯3 in the graph). In the same manner, the other two beams can be generated by successively switching OFF each element (P1 and P2 in Fig. 1*b* and each beam shown as symbol ♯1 and ♯2 in Fig. 13, respectively). The beam switching technique will be explained theoretically by using a simple point source model in following Section.

To simplify the mechanism of beam generation of a circularly polarised patch array antenna, as shown in Fig. 3, the element of patch array antenna is defined as a point source. The point source are set with sequential angle 120° to each other, or point sources P1, P2 and P3 are put on $Az = 90^\circ$, 210° and 330°, respectively. The distance between P1 and P2 is supposed as l. Hence, each point source has different phase (phase error) 120° spatially to the other elements, although the point sources are fed by the same phase. Hence, in this paper, this turning angle can be modelled as phase error of each point source.

In this paper, let us consider that the point sources P1 and P2 are turned ON and P3 is turned OFF. Current mode to the generation of circular polarisation at surface P1 is assumed as M1 and M2, and at surface P2 is M1′ and M2′. Hence, the current mode at the surface of P2 (M1′ and M2′) is rotated 120° compared with the current mode at the surface of P1 (M1 and M2), respectively. When P1 and P2 are fed by the same phase, the left-handed circular polarisation of P2 has phase error 120° compared to P1. If a straight line is drawn from P1 to P2 (weight point of each equilateral triangular patch), then, projecting this line to the co-ordinate system of Fig. 3, the line with azimuth angle $Az = 240^\circ$ will be found.

Let us define E_o, ξ_1, r', r and k_o as, respectively, amplitude (P1 and P2), phase error between P2 and P1, vector unit of P2, vector unit to the observation point (infinite distance) and wave number in free space. Here, the point of view of observation point, P2 is located $r \cdot r'$ in front of P1. Then, by referring to the patch array configuration (see Fig. 3), ξ_1 is obtained as 120°. Finally, by considering the elevation angle El and azimuth angle Az (see Fig. 3), the array factor $A(r)$ of this model can derived as

$$A(r) = E_o(1 + e^{j(\xi_1 + k_o(l \cos El \cos Az))}) \quad (1)$$

In this paper, the targeted elevation angle El is set to 48° (Tokyo area), then by considering the antenna configuration in Fig. 1*b*, the distance l between P1 and P2 is obtained as $0.58\lambda_o$, where λ_o is the wavelength in free space and $f = 2.5025$ GHz. Finally, the normalised gain of point source model (P3 is turned OFF) against Az is acquired as shown in Fig. 4. This Figure shows that the main beam is generated to $Az = 240^\circ$ and the side lobe about -6 dB at $Az = 60^\circ$. The normalised gain of MoM is employed to confirm the result of point source model. Figure 5 proves that the proposed simple point source model can describe the mechanism of beam generation of the developed antenna, where the main beam of this model matches well to the MoM ($c = 10$ mm and $f = 2.5025$ GHz). The side lobe of this point source model is lower than the MoM. We consider the influences of the groundplane size and the effect of the source model as an ideal point source or without the surface of an element. In the same manner, the beam of turned-OFF P1 or P2 can be derived by this simple model. Additionally, right-handed circular polarisation (RHCP) also can be derived by considering the opposite

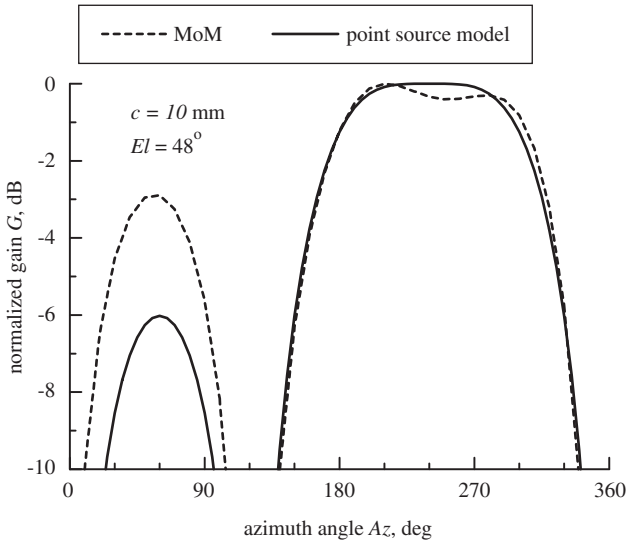

Fig. 4 *Normalised gain of MoM against point source model* $f = 2.5025$ GHz, $El = 48^\circ$

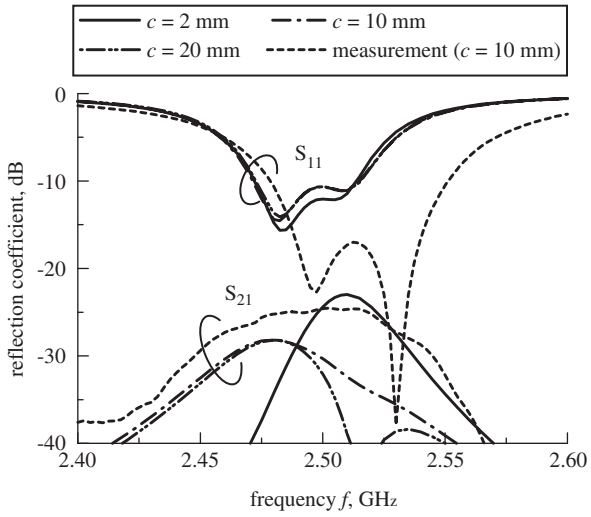

Fig. 5 *Reflection coefficient against frequency*

phase error ($-120°$). The circularly polarised array antenna with patch number more than three elements also can be derived easily by using this point source model.

3 The antenna characteristics in array configuration

In this study, the characteristics of the antenna in array configuration are discussed by studying the influence of the distance between the patch apex and the centre of the array antenna (c) in Fig. 1*b*, including the effect of ground and substrate size. By considering the antenna configuration that must be compact and satisfies the target, c is varied from 2 mm to 20 mm (the ground and the substrate size l_{sb} changes from 190 mm to 237 mm) with 2 mm interval. Then, to simplify the graph in discussion, the results of antenna models with $c = 2$ mm, 10 mm and 20 mm only (or diameter l_{sb} 190 mm, 211 mm and 237 mm) are chosen. The measurement result is appear in Figs. 5–13, where a detailed explanation will be discussed in the following Section.

Figure 5 shows the relationship between S parameters or reflection coefficients (patch number 3) and the frequency of each model when c is varied. This result shows that when the distance c or the ground and substrate size l_{sb} is increased, the reflected coefficient increases and the isolation between patch 1 and 3 improves. It is clearly caused by reduction of coupling between one patch to each other.

The S parameters (S_{11}) or reflection coefficient of the simulation model ($c = 10$ mm) using MoM for element number 3 (as shown in Fig. 1*b* or Rx3) is confirmed by measurement result ($c = 10$ mm) as represented in Fig. 5. This Figure shows that the simulation result is shifted of 0.7% to the lower frequency, from the measurement result. It is considered that the measurement systems (i.e. cable, connectors, plastic screws etc.) affect the characteristics of the antenna [14–20]. Then the isolation ($-S_{21}$) of the patches (e.g. Rx1 to Rx3 in Fig. 1*b*) is higher than 24 dB. This shows that the measurement result satisfies the target described in Table 1 and the frequency band of ETS-VIII is covered by the proposed antenna. This Figure also shows that the simulation results are shifted of 0.7% to the lower frequency, from the measurement result.

The above mentioned reason could be explained for the influence of groundplane or substrate size to the input impedance as shown in Fig. 6, respectively. The input impedance characteristic of simulation and measurement results

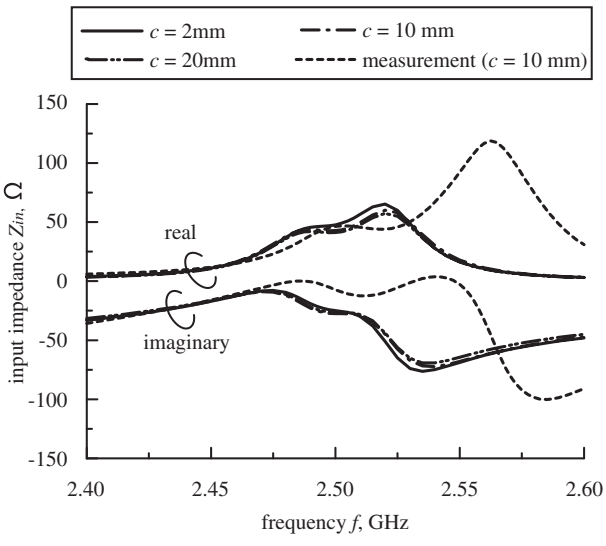

Fig. 6 *Input impedance against frequency*

($c = 10$ mm) (patch number 3) is shown in this Figure. This Figure shows that the simulation result shifts 0.7% to lower frequency than the measurement ($c = 10$ mm). The real part of measurement at targeted frequency (2.5025 GHz) is 50 Ω or matches well as the input impedance. The mismatch between measured and simulated impedance is caused by the influence of fabricating error, connector, coaxial cable, aluminium block and plastic screws to support the substrate to be flat. Empirically, these are very sensitive to the performance of the antenna, especially the input impedance.

Figure 7 shows the relationship between gain and frequency for $c = 2$ mm 10 mm and 20 mm at the peak of the beam when patch number 3 is turned off or the beam is directed towards an azimuth angle $Az = 240°$. Then the elevation angle El is set to 48°, i.e. it is adjusted to the elevation angle of ETS-VIII seen in the Tokyo area. This Figure shows that the increasing of c decreases the gain in the peak, in particular the gain of $c = 20$ mm is 1 dB lower than the gain of $c = 10$ mm.

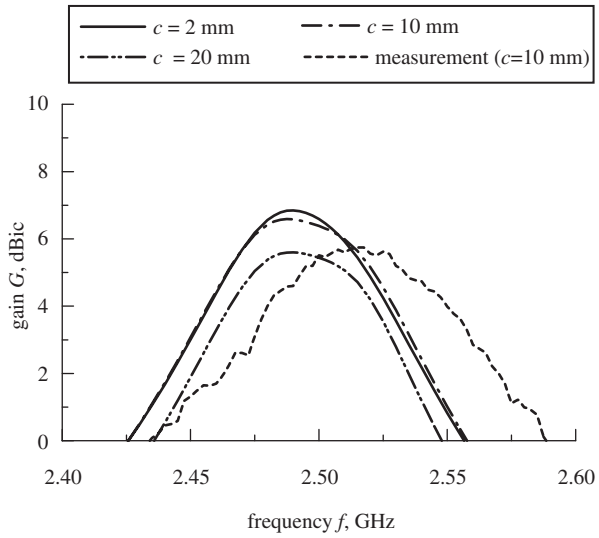

Fig. 7 *Gain against frequency*
$El = 48°$, $Az = 240°$

Based on the simulation and measurement results ($c = 10$ mm) as shown in Figs. 7 and 10, the maximum gain and the minimum axial ratio of the antenna obtained are 6.6 dBic and 0.5 dB ($f = 2.4900$ GHz), respectively, for simulation, and 5.7 dBic and 0.5 dB, respectively, for measurement ($f = 2.5025$ GHz). The measurement results show that the gain and axial ratio characteristics are satisfy the targeted performance of the frequency bands. However, the simulation results show that the minimum gain of the antenna is 0.7% to the lower frequency of the measurement result. This is due to the effect of groundplane size, hole in substrate, connector, coaxial cables etc. Additionally, the maximum gain of measurement is 0.9 dB lower than the simulation, because the loss of the measurement system, i.e. the loss of semi-rigid, connector, power divider etc. Finally, the frequency of minimum axial ratio is used to derive the antenna performance as discussed in the following Section.

Figure 8 shows the relationship between gain and azimuth angle (Az) for $c = 2$ mm, 10 mm and 20 mm at $El = 48°$. The result shows that the 5 dBic beamwidths for $c = 2$ mm, 10 mm and 20 mm are 120°, 130° and 130°, respectively. The saddle-shape beam, as shown in Fig. 8 influences the gain in the main beam which decreases when

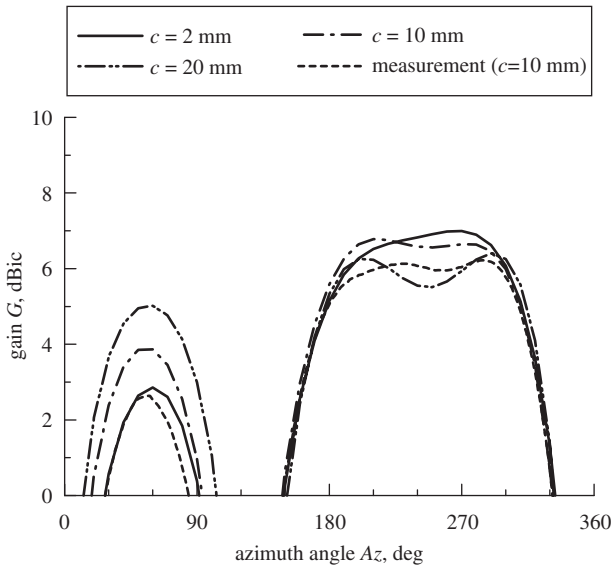

Fig. 8 *Gain against azimuth angle (El = 48°): simulation f = 2.4900 GHz and measurement f = 2.5025 GHz*

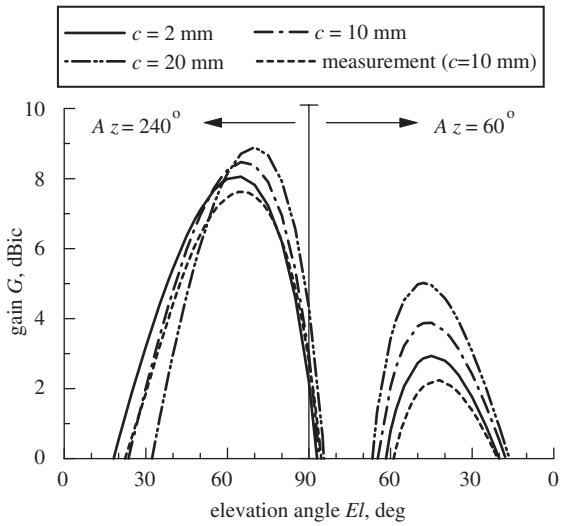

Fig. 10 *Gain against elevation angle (Az = 240°): simulation f = 2.4900 GHz and measurement f = 2.5025 GHz*

c is increased. The saddle-shape beam is generated by patches that are turned on and have a large distance between each other. This Figure also shows that increasing of c influences increasing of side lobe. The beams of all the models satisfy the target and have a beam wider than 120° for the three-patch array, hence covering the whole azimuth angle.

The 5 dBic gain beamwidths of the simulation and measurement ($c = 10$ mm) are 130° and 128°, respectively. Then the relationship between axial ratio and Az is shown in Fig. 9. This Figure shows that the 3 dB axial ratio beamwidths of simulation and measurement are 140° and 148°, respectively. Figures 8 and 9 show that the 5 dBic gain beamwidths and the 3 dB axial ratio of fabricated antenna can cover the target, and each switched beam is wider than 120°. The beam switching of the fabricated antenna by employing these results will be discussed in Section 4.

The relationship between gain and elevation angle (El) is shown in Fig. 10. This Figure shows that the increasing of c sharpens the beam, or reduces the 5 dBic gain beamwidth, and tilts the peak of the beam to the high elevation angle. Hence, the 5 dBic beamwidth covers 42°, 40° and 37° for $c = 2$ mm, 10 mm and 20 mm, respectively, and the peak of the beam is directed to $El = 65°$, 65° and 70°, respectively. This Figure also shows that the increasing of c increases the side lobe. This effect is considered to be due to the influence of increasing the size of ground and substrate [14].

If the antenna is put on a car roof and the shaking of the car is considered to be $\pm 10°$ in the elevation angle with centre at $El = 48°$, the gain and axial ratio in this range must satisfy the targets (minimum gain 5 dBic and maximum axial ratio 3 dB). Figures 10 and 11 show that the minimum gains of simulation result ($c = 10$ mm) between $El = 40°$ to 58° are higher than 5 dBic, and the measurement result ($c = 10$ mm) covers $El = 42°$ to 58°. Additionally, the maximum axial ratios of both simulation and measurement at $El = 38°$ to 58° are lower than 3 dB. This Figure shows that the axial ratio satisfies the targets, and the gain at low elevation angle needs an improvement of 2° and 4° coverage for simulation and measurement, respectively. The reason discussed in the preceding paragraph can also be employed to explain this phenomenon.

Then Fig. 12 shows the relationship between axial ratio and frequency for $c = 2$ mm, 10 mm and 20 mm at $Az = 240°$ and $El = 48°$. This Figure shows that the

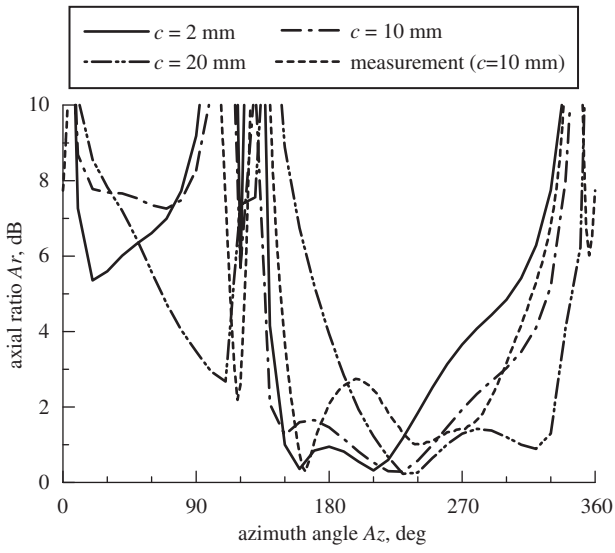

Fig. 9 *Axial ratio against azimuth angle (El = 48°): simulation f = 2.4900 GHz and measurement f = 2.5025 GHz*

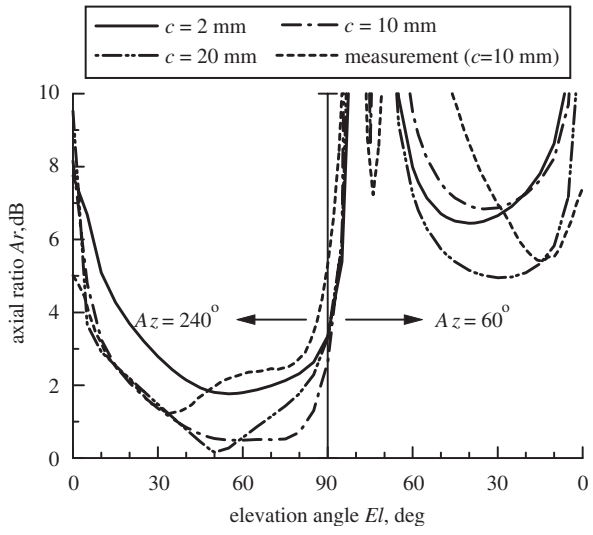

Fig. 11 *Axial ratio against elevation angle (Az = 240°): simulation f = 2.4900 GHz and measurement f = 2.5025 GHz*

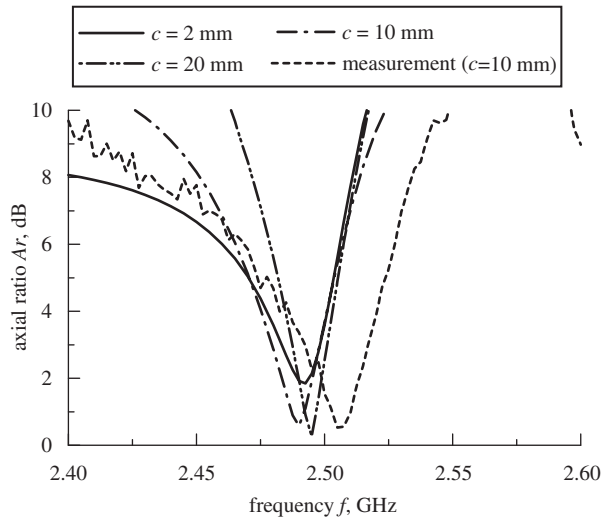

Fig. 12 *Axial ratio against frequency*
El = 48°, *Az* = 240°

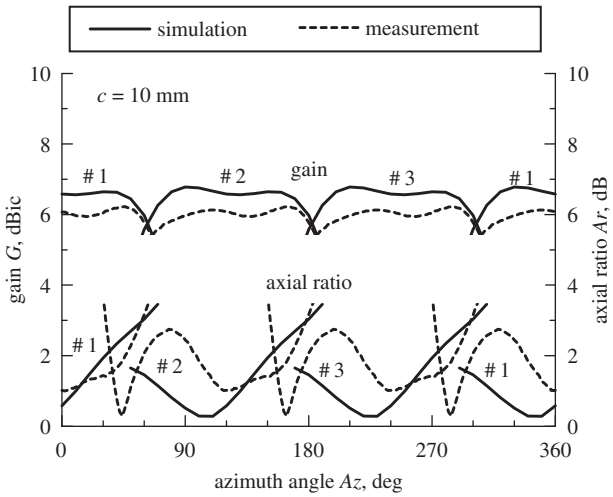

Fig. 13 *Radiation characteristics in the conical-cut plane (El = 48°): simulation f = 2.4900 GHz and measurement f = 2.5025 GHz*

bandwidth of 3 dB axial ratio is 0.6%, 0.7% and 0.5% for $c = 2$ mm, 10 mm and 20 mm, respectively. The result shows that the patch array with $c = 10$ mm has the widest bandwidth.

Figure 9 shows the relationship between axial ratio and *Az*. This Figure shows that the 3 dB axial ratio beamwidth is 110°, 140° and 130°, for $c = 2$ mm, 10 mm and 20 mm, respectively. This result shows that the 3 dB axial ratio beamwidth of $c = 10$ mm has the widest coverage. In the case of $c = 20$ mm, the axial ratio beamwidth is shifted compared to the 5 dBic gain beamwidth shown in Fig. 8. This shifting is considered due to the effects decreasing the gain in the main beam direction (saddle-shape beam), as shown in Fig. 8.

The relationship between axial ratio and elevation angle *El* is shown in Fig. 11. The 3 dB axial ratio coverage of $c = 2$ mm, 10 mm and 20 mm is 55°, 75° and 75°, respectively. This result shows that the closed configuration of the patch array will generate a strong coupling inside the antenna configuration, and it influences the characteristics of the antenna, especially the axial ratio.

Based on these results, the distance of the patch apex to the centre of antenna (c) is selected as 10 mm, in other words, the diameter of model l is set to 211 mm. Then the diameter l_{sb} of substrate and groundplane for the fabricated antenna is set to 210 mm or 1 mm smaller than the simulated antenna. Confirmation of simulation and measurement (both $c = 10$ mm) is discussed in the Section 4.

4 Verification of beam switching

The simulation and measurement results ($c = 10$ mm) of gain and axial ratio characteristics of the beams switching in the conical-cut plane are shown in Fig. 13. The Figure shows the maximum gain is 5.8 dBic and 5.4 dBic by simulation and measurement, respectively. The result shows that both simulation and measurement results are satisfied, or these results are greater than the target (minimum gain 5.0 dBic) and cover the whole azimuth angle (the 5 dBic beam coverage is wider than 120°).

The obtained minimum axial ratios for simulation and measurement, as shown in Fig. 13, are 3.1 dB and 3.4 dB, respectively. The 3 dB axial ratio coverage of simulation and measurement results cover 354° and 351° in a conical-cut plane at *El* = 48°.

Figure 13 shows the saddle-shape beam pattern is occurring for the main beam of gain and axial ratio. The beam pattern in the main beam is strongly generated when the distance between the centre of the antenna and the apex of the patch is reduced [8] or the distance decreased. This effect is also considered to induce a decrease in antenna performance, especially the axial ratio. This is considered to be due to the influence of the edge effect that generates an oscillation of current distribution on the surface of the patch with finite groundplane, or when the substrate surface is reduced, therefore changing the antenna characteristics, especially the resonant frequency (see Fig. 5) and radiation patterns [14–20].

5 Conclusions

JAXA will launch ETS-VIII in 2006 to conduct orbital experiments on mobile satellite communications at the *S* band frequency. Hence, a circularly polarised simple satellite-tracking dual-band triangular-patch array antenna for mobile satellite communications aiming at ETS-VIII applications has been developed in this research. The simple point source model was proposed to describe the beam generation, then MoM is employed to design the antenna and investigate the characteristics of patches in array configuration, then measurement of the fabricated antenna was performed to confirm the simulation results. The result of the point source model and MoM shows a match-well switched beam.

The developed antenna with $c = 10$ mm is thin, small, simple and compact compared to previous antennas, and has stable switching able to generate beams that can cover the azimuth angles. Moreover, the performance of the antenna satisfies the targeted specification. This is considered to be due to the influence of edge effects and the measurement system.

In following research, the dual-band antenna configuration in the array configuration will be designed for reception (frequency 2.5025 GHz band) and transmission (frequency 2.6575 GHz band), then the optimisation of antenna parameters by considering the edge effects in a finite groundplane can be done. The improvement of feed type (microstripline) for a circularly polarised triangular-patch antenna may also be developed to enhance the isolation between transmission and reception, then the generation of the beam that has the main direction at low elevation angle may also be considered in future research to improve the

performance of the antenna that will be used at the Tokyo area (centre direction of elevation angle $El = 48^\circ$).

6 Acknowledgments

The authors thank the Japan Society for the Promotion of Science (JSPS) for Grant-in-Aid for Scientific Research (Project 16360185).

7 References

1 Jang, J.H., Tanaka, M., and Hamamoto, N.: 'Portable and deployable antenna for ETS-VIII'. Proc. Interim Int. Symp. Antennas Propagation, 2002, pp. 49–52
2 Ito, K., Ohmaru, K., and Konishi, Y.: 'Planar antennas for satellite reception', *IEEE Trans. Broadcast.*, 1988, **34**, pp. 457–464
3 Ito, K., Daniel, J-P., and Lenormand, J-M.: 'A printed antenna composed of strip dipoles and slots generating circularly polarised conical patterns'. Proc. IEEE AP-S Int. Symp., 1989, pp. 632–635
4 Fujimoto, K., and James, J.R.: 'Mobile antenna systems handbook' (Artech House, Boston, 1994)
5 Nakano, M., Arai, H., Chujo, W., Fujise, M., and Goto, N.: 'Feed circuits of double-layered self-diplexing antenna for mobile satellite communications', *IEEE Trans. Antennas Propaga.*, 1992, **40**, pp. 1269–1271
6 Ishihara, H., Yamamoto, A., and Ogawa, K.: 'A simple model for calculating the radiation patterns of antennas mounted on a vehicle roof'. Proc. Interim Int. Symp. Antennas Propagation, 2002, pp. 548–551
7 Sri Sumantyo, J.T., Ito, K.: 'Simple satellite-tracking triangular-patch array antenna for ETS-III applications', *Radiomatics, J. Commun. Eng.* (in press)
8 Sri Sumantyo, J.T., Ito, K., Delaune, D., Tanaka, T., and Yoshimura, H.: 'Simple satellite-tracking dual-band triangular-patch array antenna for ETS-VIII applications'. Proc. IEEE AP-S Int. Symp., 2004, pp. 2500–2503
9 Lu, J.H., and Wong, K.L.: 'Singly-fed circularly polarised equilateral-triangular microstrip antenna with a tuning stub', *IEEE Trans. Antennas Propag.*, 2002, **48**, pp. 1869–1872
10 Suzuki, Y., Miyano, N., and Chiba, T.: 'Circularly polarised radiation from singly-fed equilateral-triangular microstrip antenna', *IEE Proc. H, Microw. Antennas Propag.*, 1987, **134**, pp. 194–198
11 Garg, R., Bhartia, P., Bahl, I., and Ittipiboon, A.: 'Microstrip antenna design handbook' (Artech House, Boston, London, 2001)
12 James, J.R., and Hall, P.S.: 'Handbook of microstrip antennas' (Peter Peregrinus, 1989)
13 Kumar, G., and Ray, K.P.: 'Broadband microstrip antennas' (Artech House, Boston, 2003)
14 Sri Sumantyo, J.T., Ito, K., Delaune, D., Tanaka, T., Onishi, T., and Yoshimura, H.: 'Numerical analysis of ground plane size effects on patch array antenna characteristics for mobile satellite communications', *Int. J. Numer. Model. Electron. Netw. Devices Fields*, 2005, **18**, (2), pp. 95–106
15 Otero, M.F., and Rojas, R.G.: 'Analysis and treatment of edge effects on the radiation pattern of a microstrip patch antenna'. Proc. IEEE AP-S Int. Symp., 1995, pp. 1050–1053
16 Lier, E., and Jacobsen, K.: 'Rectangular microstrip patch antennas with infinite and finite ground plane dimensions', *IEEE Trans. Antennas Propag.*, 1983, **31**, pp. 978–984
17 Delgado, H.J., Williams, J.T., and Long, S.A.: 'Substraction of edge-diffracted fields in antenna radiation pattern for simulation of infinite ground plane', *Electron. Lett.*, 1989, **25**, pp. 694–696
18 Iyer, S.M.V., and Karekar, R.N.: 'Edge effects for resonance frequency of covered rectangular microstrip patch antenna', *Electron. Lett.*, 1991, **27**, pp. 1509–1511
19 Maci, S., and Borselli, L.: 'Diffraction at the edge of a truncated grounded dielectric slab', *IEEE Trans. Antennas Propag.*, 1996, **44**, pp. 863–873
20 Maci, S., Borselli, L., and Cucurachi, A.: 'Diffraction from a truncated grounded dielectric slab: A comparative full-wave/physical-optics analysis', *IEEE Trans. Antennas Propag.*, 2000, **48**, pp. 48–57